Distinct signaling of *Drosophila* chemoreceptors in olfactory sensory neurons

Li-Hui Cao[a,b,c,d], Bi-Yang Jing[a,b,c,d,1], Dong Yang[e,1], Xiankun Zeng[f,1], Ying Shen[e], Yuhai Tu[g], and Dong-Gen Luo[a,b,c,d,2]

[a]State Key Laboratory of Membrane Biology, College of Life Sciences, Peking University, Beijing 100871, China; [b]Center for Quantitative Biology, Peking University, Beijing 100871, China; [c]McGovern Institute for Brain Research, Peking University, Beijing 100871, China; [d]Peking–Tsinghua Center for Life Sciences, Academy for Advanced Interdisciplinary Studies, Peking University, Beijing 100871, China; [e]Department of Neurobiology, Zhejiang University School of Medicine, Hangzhou 310058, China; [f]Janelia Research Campus, Howard Hughes Medical Institute, Ashburn, VA 20147; and [g]IBM T. J. Watson Research Center, Yorktown Heights, NY 10598

Edited by Richard W. Aldrich, The University of Texas at Austin, Austin, TX, and approved December 24, 2015 (received for review September 15, 2015)

In *Drosophila*, olfactory sensory neurons (OSNs) rely primarily on two types of chemoreceptors, odorant receptors (Ors) and ionotropic receptors (Irs), to convert odor stimuli into neural activity. The cellular signaling of these receptors in their native OSNs remains unclear because of the difficulty of obtaining intracellular recordings from *Drosophila* OSNs. Here, we developed an antennal preparation that enabled the first recordings (to our knowledge) from targeted *Drosophila* OSNs through a patch-clamp technique. We found that brief odor pulses triggered graded inward receptor currents with distinct response kinetics and current–voltage relationships between Or- and Ir-driven responses. When stimulated with long-step odors, the receptor current of Ir-expressing OSNs did not adapt. In contrast, Or-expressing OSNs showed a strong Ca^{2+}-dependent adaptation. The adaptation-induced changes in odor sensitivity obeyed the Weber–Fechner relation; however, surprisingly, the incremental sensitivity was reduced at low odor backgrounds but increased at high odor backgrounds. Our model for odor adaptation revealed two opposing effects of adaptation, desensitization and prevention of saturation, in dynamically adjusting odor sensitivity and extending the sensory operating range.

Drosophila | olfaction | chemoreceptor | sensory adaptation | OSN

From insects to mammals, the sense of smell begins with odor detection by olfactory sensory neurons (OSNs) (1–6). Recently, rapid advances have been made in understanding chemoreceptors in *Drosophila* OSNs (7–9). To date, *Drosophila* is the only model organism for which odor selectivity is known for most of its odorant receptors (Ors) (10, 11), and an Or expression pattern has been mapped to OSNs (12, 13). In addition, another family of chemoreceptors called ionotropic receptors (Irs) has been identified and characterized (14–16). These two types of chemoreceptors respond to different odors, thus endowing *Drosophila* OSNs with unique and complementary properties for odor detection (17). In contrast to the advanced molecular understanding of these two types of chemoreceptors, the mechanisms of their cellular signaling in native OSNs remain unclear, particularly hampered by the technical difficulty of carrying out patch-clamp recordings of *Drosophila* OSNs.

Drosophila OSNs are encased in hair-like sensilla in the antennae and maxillary palps, with each sensillum containing the dendrites of one to four OSNs that are wrapped by sheath cells (18). The responses of native *Drosophila* OSNs to odors have traditionally been measured by electroantennogram (EAG) (19), which extracellularly measures the potentials across the entire antenna. In addition, single-sensillum recording (SSR) was developed to provide a higher spatial resolution by measuring the local field potentials (LFPs) from a single sensillum (20–24). These methods, especially SSR, have greatly advanced understanding of the odor selectivity of both Ors and Irs (10, 11, 14). However, because sheath cells and other OSNs also contribute to EAG and SSR signals (25), the response characteristics obtained by such measurements are often contaminated. Patch-clamp recordings of single OSNs could ideally overcome this issue while facilitating the experimental manipulations of a cell's membrane potential; however, this standard method has unfortunately not yet been routinely applied to *Drosophila* OSNs.

Here, we developed a *Drosophila* antennal preparation and succeeded in performing patch-clamp recordings of single identified OSNs. By using a fast solution change system to deliver liquid-phase odor stimuli, we investigated the response properties of odor-induced receptor currents of *Drosophila* OSNs. We found that OSNs expressing Ors exhibited slow response kinetics, outward receptor current rectification, and strong adaptation to odors. We further demonstrated that this adaptation was produced by a Ca^{2+} influx into OSNs because it could be eliminated by voltage clamping at positive holding potentials, by removing extracellular Ca^{2+}, or by removing internal free Ca^{2+} with a Ca^{2+} chelator 1,2-bis(2-aminophenoxy)ethane-*N*, *N*,*N*′,*N*′-tetraacetic acid (BAPTA). Importantly, in contrast to the long-held view that adaptation simply increases sensitivity, we found that Or-mediated adaptation selectively reduced odor-signaling gain at low odor backgrounds but increased the gain at high odor backgrounds, thereby extending the dynamic odor-operating range. In contrast, odor-induced receptor currents in Ir-expressing OSNs showed fast response kinetics and, surprisingly, did not adapt.

Significance

***Drosophila* is a popular model system for the study of olfaction. However, the physiological properties of its olfactory sensory neurons, both intrinsic and responsive, remain unclear. We have succeeded, for the first time, in patch-clamp recording from targeted *Drosophila* OSNs, revealing the distinct signaling of odorant receptors (Ors) and ionotropic receptors (Irs). We found that Ir-driven receptor currents did not adapt, whereas Or responses strongly adapted. Surprisingly, although Or adaptation increased odor sensitivity at high odor backgrounds, it reduced odor sensitivity at low backgrounds. Adaptation permeates all senses, and the finding of dynamic gain control by adaptation in *Drosophila* Or-expressing OSNs sheds light on the understanding of adaptation in other sensory systems.**

Author contributions: L.-H.C. and D.-G.L. designed research; L.-H.C., Y.T., and D.-G.L. developed the adaptation model; L.-H.C., B.-Y.J., D.Y., X.Z., and D.-G.L. performed research; L.-H.C., B.-Y.J., D.Y., Y.S., and D.-G.L. analyzed data; and L.-H.C., Y.T., and D.-G.L. wrote the paper.

The authors declare no conflict of interest.

This article is a PNAS Direct Submission.

[1]B.-Y.J., D.Y., and X.Z. contributed equally to this work.

[2]To whom correspondence should be addressed. Email: dgluo@pku.edu.cn.

This article contains supporting information online at www.pnas.org/lookup/suppl/doi:10.1073/pnas.1518329113/-/DCSupplemental.

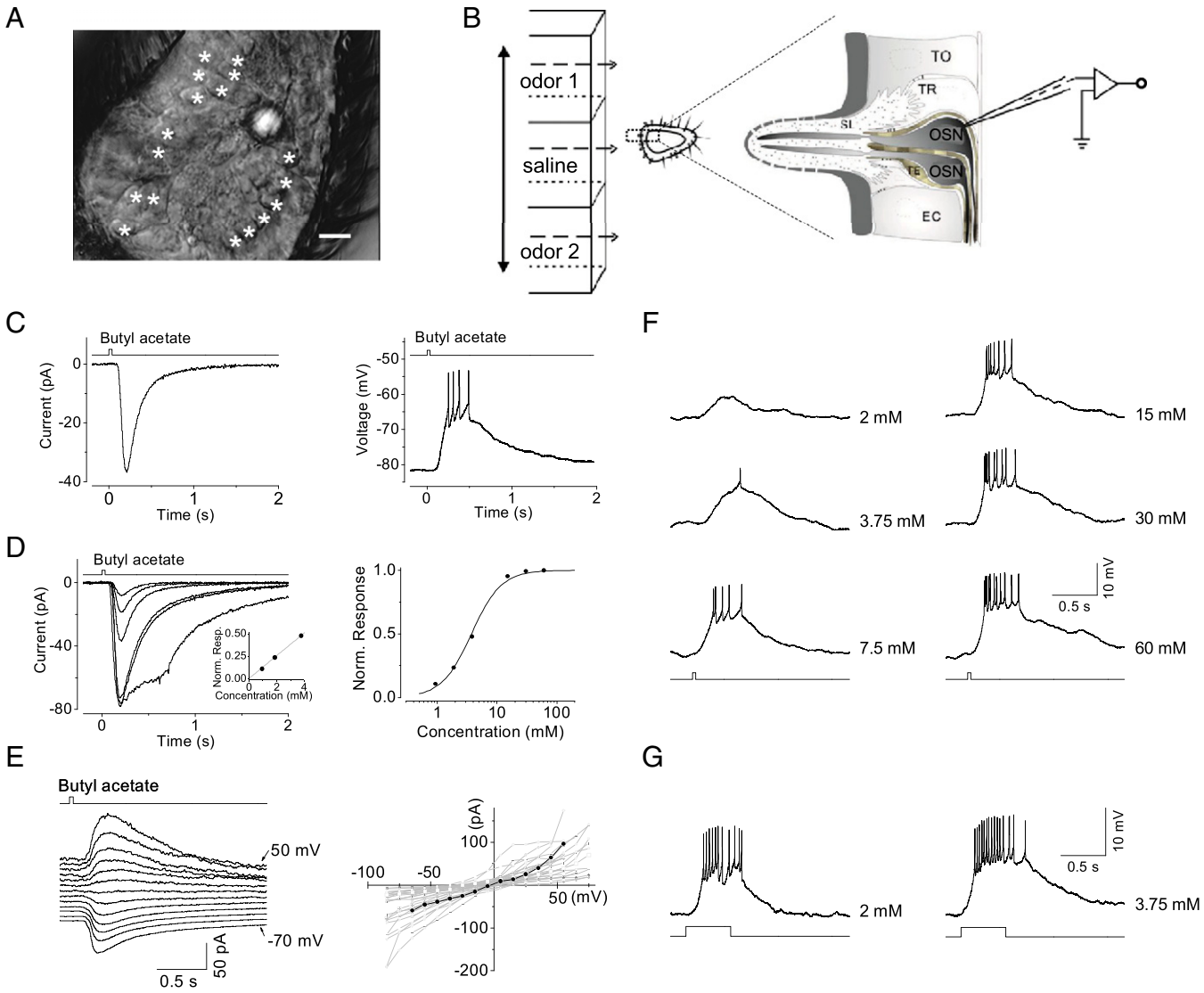

Fig. 1. Odor responses of Or-expressing OSNs. (*A*) Infrared–differential interference contrast (IR-DIC) image of an antennal slice. The third segment of an antenna was transversely cut into three slices (*Materials and Methods*). The antennal slice was stabilized on the recording chamber, with one cutting end facing up and all sensilla pointing horizontally. The OSN cell bodies, marked by asterisks, are exposed. (Scale bar: 5 μm.) (*B*) Odor stimulation and recording arrangement. A three-barrel array, moved horizontally by a stepper, is placed ∼50 μm away from the antennal slice, with the middle barrel containing *Drosophila* saline and the flanking barrels containing odor solutions. The expanded diagram on the right illustrates a patch-clamp recording of an OSN. EC, epithelium cell; SL, sensillum lymph; TE, thecogen cell; TO, tomorgen cell; TR, trichogen cell. (*C*, *Left*) Inward receptor current recorded under voltage clamping (−82 mV) and a 35-ms pulse of 4 mM butyl acetate. (*Right*) The same response as that on the *Left* but under current clamping, showing action potential firing. (*D*, *Left*) A family of superimposed responses to a 35-ms pulse of butyl acetate at 1, 2, 4, 15, 30, and 60 mM. This is the same cell as that shown in *C*. Each trace is the average of three to five trials. (*Right*) The normalized dose–response relationship of the response family on the *Left*. The curve is the Hill equation, $R/R_{max} = C^m/(C^m + K_{1/2}{}^m)$, where R is the response amplitude at the transient peak, R_{max} is the maximum (i.e., saturated) response, C is the odorant concentration, $K_{1/2}$ is the odor concentration that half-saturates the response, and m is the Hill coefficient. In this experiment, $K_{1/2} = 3.7$ mM, $m = 1.7$. The *Inset* shows that the relationship is actually linear at its foot. (*E*, *Left*) The current–voltage relationship of the butyl acetate-elicited response. The cell was voltage clamped at −70 mV and then stepped to the indicated voltages in 10-mV increments. Odor stimulation: 35-ms pulses of 15 mM butyl acetate. (*Right*) Collective relationships of 34 Or-expressing OSNs indicate moderate outward rectification, with a reversal potential of −9 ± 13 mV (mean ± SD). Black dots (interconnected by straight lines) correspond to data from the OSN on the *Left*. (*F*) Dose dependence of spike firing. The traces show the membrane depolarization (current clamped) induced by brief (35-ms) pulses of butyl acetate at concentrations of 2, 3.75, 7.5, 15, 30, and 60 mM. The resting membrane potential was −73 mV. (*G*) Temporal integration of the odor response. The same cell produces no spike firing in response to the 35-ms, 2 mM butyl acetate stimulus in *F* but fires robustly in response to the 500-ms, 2 mM butyl acetate and fires even more robustly to 500-ms, 3.75 mM butyl acetate. In each panel, the top trace (*C*–*E*) and bottom trace (*F* and *G*) indicate the timing of the voltage trigger controlling the solution change (see Fig. S1 legend for details). *C and D* from the same OSN; *E* from another OSN; and *F* and *G* from yet another OSN.

Results

Patch-Clamp Recordings of Odor Responses in Or-Expressing OSNs. *Drosophila* OSNs are bipolar neurons, each with a single chemosensitive dendrite protruding into a small, hair-like sensillum covered by a cuticle. In the antenna, ∼80% of the total 1,200 OSNs are Or-expressing OSNs that coexpress Orco and odorant-binding Ors (12, 13, 26), the former of which is a coreceptor present in all Or-expressing OSNs (26). We have succeeded in developing an antennal-slice preparation (Fig. 1*A* and *Materials and Methods*) that allows perforated-patch recording of a genetically labeled OSN. OSNs were identified by expressing mCD8-GFP via a binary Gal4/UAS expression system in *Orco-Gal4* flies

Table 1. Parameters of odor-induced receptor currents

OSN types	R_{max}, pA	$t_{latency}$, ms	t_{peak}, ms	t_{rise}, ms	t_{int}, ms	Cell no.
Orco-expressing OSNs (in situ)	−51 ± 31	66 ± 25	138 ± 42	62 ± 23	250 ± 103	25
Ir-expressing OSNs (in situ)	−49 ± 35	35 ± 16	104 ± 25	52 ± 14	225 ± 106	10
Or47a-expressing OSNs (in situ)	−94 ± 53	67 ± 35	132 ± 46	55 ± 24	275 ± 86	10
Or47a-expressing OSNs (dendrite out)	−103 ± 65	64 ± 36	128 ± 45	53 ± 18	251 ± 79	5
Or22a-expressing OSNs (in situ)	−63 ± 36	65 ± 17	135 ± 23	58 ± 21	246 ± 65	15

Note: R_{max} is the transient-peak amplitude of the saturated odor response. Integration time of odor response, t_{int}, is defined as $\int f(t)dt/f_p$, where $f(t)$ is the response waveform and f_p is the waveform's transient-peak amplitude. Other parameters are defined in Fig. S1*H*. All data are given as mean ± SD, derived from responses filtered at DC-2 kHz.

(Fig. S1 *A–C*). With a stepper-driven, rapid solution-switching system to translate the interface between two solution streams across the recorded cell (27), we were able to apply brief and precise odor pulses to the recorded OSNs (Fig. 1*B*). The OSNs appeared healthy and remained healthy with a stable membrane potential for up to 2 h. Under cell-attached recordings, the OSNs showed a strong firing ability similar to that observed for the in vivo SSR preparation (Fig. S1*D*). For the odor stimulus, we typically used butyl acetate, a common fruit odor that activates many Ors (11). We found that most Or-expressing OSNs in the dorsomedial part of the antenna were butyl acetate responsive (Fig. S1*E*), whereas others were poorly responsive to butyl acetate (Fig. S1*F*). In the absence of the Orco protein (26), we found that these OSNs lost their odor responses completely.

In Fig. 1*C*, *Left*, a brief (35-ms) pulse of 4 mM butyl acetate elicited an inward current of approximately −40 pA from a representative, voltage-clamped Or-expressing OSN. Across cells, the saturated response ranged from −20 to −160 pA (−51 ± 31 pA, mean ± SD; $n = 25$). The response amplitude increased with increasing concentration (Fig. 1*D*, *Left*), with a dynamic range covering 1–2 log units of butyl acetate concentration (Fig. 1*D*, *Right*). The dose–response relationship was approximately linear at its foot (Fig. 1*D*, *Left*, *Inset*) but was supralinear overall (Hill coefficient, 1.7 for this cell), broadly similar to the behavior of vertebrate OSNs (27, 28). As expected from OSNs expressing different Ors, the sensitivity to butyl acetate varied widely across randomly recorded Or-expressing OSNs, with a half-saturating concentration of 0.6–17 mM (10 cells; 3.7 mM in Fig. 1*D*) for 35-ms pulses, but the Hill coefficient was fairly constant (1.5 ± 0.3; $n = 10$). The receptor current elicited by butyl acetate showed a moderate outward rectification in the physiological voltage range with a reversal potential of −9 ± 13 mV ($n = 34$) (Fig. 1*E*), suggesting the involvement of a nonselective transduction cation channel.

Under current clamping, the responsive OSNs depolarized to generate action potentials, yielding higher firing frequencies at higher odor concentrations (Fig. 1*F*). When the duration of odor simulation was prolonged to 500 ms, the same recorded OSN responded strongly with a high firing frequency (Fig. 1*G*, *Left*) to butyl acetate at 2 mM, a concentration that did not trigger any firing with a 35-ms pulse (Fig. 1*F*). The response increased further for butyl acetate at 3.75 mM and 500 ms (Fig. 1*G*, *Right*). Thus, both the concentration and duration of odor stimulation contribute to the response strength, explaining why a brief pulse (e.g., 35 ms) requires a relatively high concentration to trigger a substantial response, as shown above. The concentrations used here do not correspond directly to those used in the air-phase odor stimulation in SSR (see *Supporting Information* for details).

To examine the response kinetics, we followed the strategy adopted for vertebrate photoreceptors by focusing on small responses at the foot of the dose–response curve, where linearity holds and intrinsic kinetics is revealed (29). The profile of the small receptor current showed a sigmoidal rise, with a latency ($t_{latency}$) of 66 ± 25 ms ($n = 25$) (i.e., time from odor arrival to 10% of response peak amplitude; Fig. S1 *G* and *H*) and a time-to-peak (t_{peak}) of 138 ± 42 ms ($n = 25$) (Table 1). The rise time (t_{rise}, from 10% to 90% of response) of the receptor current was 62 ± 23 ms ($n = 25$). The integration time of the response (t_{int}) (30), which provides a representation of the overall response duration independent of its specific waveform (Table 1 legend) and is useful for performing comparisons across OSNs and even comparisons with sensory neurons of other modalities, was 250 ± 103 ms ($n = 25$). We also found that the responses of a given OSN to different odors typically exhibited comparable rising phases but sometimes widely variable falling phases (10). The reason for this variability remains unclear.

In addition, we examined two additional *Drosophila* lines in which OSNs expressing Or22a and Or47a were GFP labeled. The odors that we found effective for these OSNs (Fig. 2 *A* and *B*) were broadly similar to those previously identified for Or22a and Or47a expressed in "empty neurons" lacking endogenous Ors (11). By using butyl acetate and pentyl acetate as the stimulus for Or22a- and Or47a-expressing OSNs, respectively, we found that these OSNs produced odor responses with similar properties to those described above (Fig. 2 *C–F*), including the maximum amplitude (Table 1), response kinetics (Table 1), and current–voltage relationship.

Next, we compared the responses of an in situ Or47a-expressing OSN (i.e., with its chemosensory dendrite inside the sensillum, corresponding to the experiments described so far) with those of an Or47a-expressing OSN with its dendrite directly exposed to the bath perfusion solution (Fig. 2*G* and *Materials and Methods*). We found that the responses under the two experimental conditions were remarkably similar (Fig. 2 *C* and *G*, and Table 1), except for the slightly higher half-saturating pentyl acetate concentration associated with the dendrite-out OSNs (in situ: 1.7 ± 1.1 mM, $n = 10$; versus dendrite-out: 2.4 ± 1.5 mM, $n = 5$). These data suggest that when pentyl acetate is applied in the liquid phase, the intrasensillar lymph is not important for odor response kinetics and sensitivity. Alternatively, a partial lymph washout or dilution may have occurred for in situ ORNs due to the continuous bath perfusion.

Odor Responses in Ir-Expressing OSNs. For comparison, we recorded Ir-expressing OSNs, which compose 20% of the total 1,200 OSNs in the antenna. To avoid any confounding Or-mediated signals, we focused on GFP-negative OSNs in *Orco-Gal4;;Orco*^{2}*, UAS-mCD8-GFP* flies, which express either Irs or the gustatory receptors Gr21a/Gr63a (16). These two subpopulations of chemoreceptive cells can be distinguished from each other by their distinct responsivities to a panel of odorants (Gr21a/Gr63a respond mainly to CO_2). In the *Orco*$^{-/-}$ background, any potential influence of a neighboring Or-expressing OSN would also be eliminated (31). Thus, we were able to record a subpopulation of Ir-expressing OSNs with a distinct odor spectrum (Fig. 3*A*) similar to that of ac3A neurons (16, 32). When stimulated with butyric acid, the OSN fired bursts of action potentials, with increasing firing frequency at higher odor concentrations (Fig. 3*B*). Under voltage clamping, an inward receptor current was elicited from these cells by butyric acid, with a peak amplitude that was graded

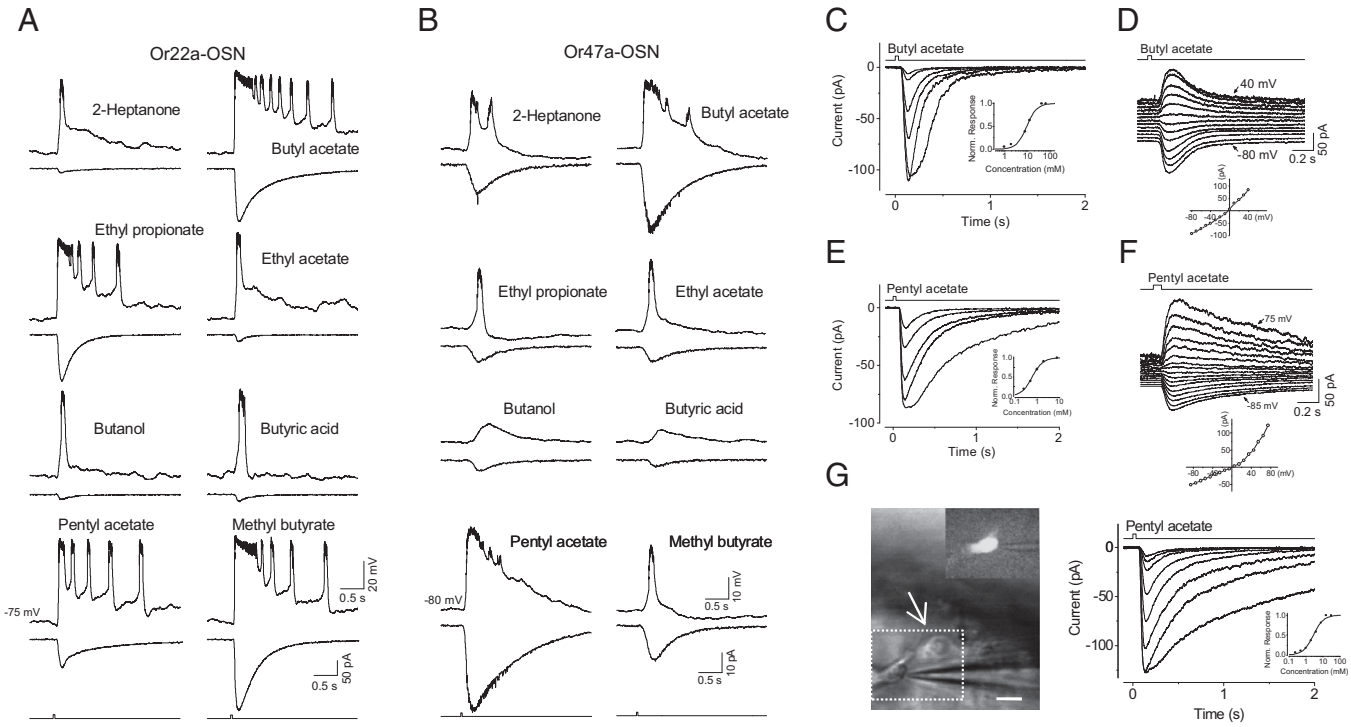

Fig. 2. Odor responses of Or22a- and Or47a-expressing OSNs. (*A*) The odor spectrum of an Or22a-expressing OSN. In each pair of traces, the top trace shows the voltage response (current clamped) and the bottom trace shows the inward receptor current (voltage clamped at −75 mV) elicited by the indicated odors (10 mM, applied for 35 ms). Each of the multiple peaks in the odor responses obtained via current-clamped recordings represents a burst of action potential firing, which also occurs in some OSNs when injected with depolarizing currents. Note the voltage trace is faster than the current trace, possibly due to the contribution of voltage-gated conductance to voltage changes. (*B*) The odor spectrum of an Or47a-expressing OSN. (*C*) The odor response family of an Or22a-expressing OSN. Odor stimulations with 35-ms pulses of butyl acetate at concentrations of 1, 2, 8, 12, 40, and 60 mM. The *Inset* shows the corresponding normalized dose–response relationship. The curve is the Hill equation ($K_{1/2}$ = 9 mM, m = 1.9). (*D*) The current–voltage relationship for the response in an Or22a-expressing OSN. The voltage is clamped at −80 mV and stepped to +40 mV in 10-mV increments. Odor stimulation: 35-ms pulses of 10 mM butyl acetate. (*E*) The odor response family of an Or47a-expressing OSN. Odor stimulations via 35-ms pulses of pentyl acetate at concentration of 0.25, 0.5, 1, 2, and 7.5 mM. The *Inset* shows the corresponding normalized dose–response relationship. The curve is the Hill equation ($K_{1/2}$ = 0.6 mM, m = 1.8). (*F*) The current–voltage relationship for the response of an Or47a-expressing OSN. The voltage is clamped at −85 mV and stepped to +75 mV in 10-mV increments. Odor stimulation: 75-ms pulses of 1 mM pentyl acetate. (*G*) Odor responses of an Or47a-expressing OSN with its dendrite exposed. (*Left*) Image of a dendrite-out OSN. The arrow indicates the exposed dendrite. The *Inset* illustrates GFP fluorescence in the dashed box region. (Scale bar: 5 μm.) (*Right*) Odor response family for the OSN on the *Left*. The *Inset* is the normalized dose–response relationship.

with concentration (Fig. 3*C*). The Hill coefficient of the overall dose–response relationship across these OSNs was 1.2 ± 0.4 (n = 10). The response to butyric acid showed an approximately linear current–voltage relationship, with a reversal potential of −11 ± 15 mV (Fig. 3*D*; n = 17). In data from 10 cells, the average $t_{latency}$, t_{rise}, t_{peak}, and t_{int} were 35 ± 16, 52 ± 14, 104 ± 25, and 225 ± 106 ms, respectively (Table 1). The key difference between Or- and Ir-expressing OSNs is the shorter $t_{latency}$ and t_{peak} of the latter, suggesting that a difference may exist in the odor signaling mechanisms of *Drosophila* Ors and Irs.

Adaptation of the Receptor Current in OSNs. To determine the adaptation of odor responses, we first recorded the responses of Or22a-expressing OSNs to a 30-s odor step. We chose ethyl propionate, a potent excitatory odor recognized by Or22a (Fig. 2*A*) with relatively high water solubility, as the stimulus. The receptor current rose to a transient peak, and then substantially decreased and was maintained a steady response in the presence of the odor step, an indicator of adaptation (Fig. 4*A*; n = 22). At higher concentrations, the amplitude of the transient peak became larger and eventually saturated. In contrast, the steady current first increased with concentrations and then decreased at the highest concentration tested, possibly due to nonspecific inhibition (33). A broadly similar adaptation was also observed with butyl acetate and pentyl acetate. To investigate the time course of recovery from adaptation, we examined responses to paired-pulse stimulations at varied interpulse intervals. At an interval of 500 ms, the second pulse induced a smaller receptor current relative to the first, indicating the existence of adaptation produced by the first pulse; at longer intervals, the reduction of the receptor current gradually recovered (Fig. 4*B*; n = 12). The presence of residual adaptation even when the response to the first pulse had already decayed to near zero suggests that the adaptation was produced by changes associated with receptor current generation.

This adaptation may be caused by perineuronal effects, such as the depletion of odorant-binding proteins or ionic concentration changes in sensillar lymph (34), or by desensitized cellular signaling intrinsic to the OSNs. To distinguish between these possibilities, we examined the adaptation of OSNs with their sensory dendrites pulled out of the sensillar cavities to preclude any perineuronal effects. Nonetheless, we observed a similar adaptation to odor steps and similar recovery kinetics associated with paired-pulse adaptation (Fig. 4 *C* and *D*; n = 6). These results demonstrated that the adaptation is produced by the desensitization of intrinsic signaling in OSNs.

Or47a-expressing OSNs also showed strong adaptation to a long step of pentyl acetate and exhibited a similar recovery from the adaptation induced by paired-pulse stimulation (Fig. S2 *A* and *B*). In addition, randomly recorded Orco-expressing OSNs also exhibited adaptation, further supporting the idea that

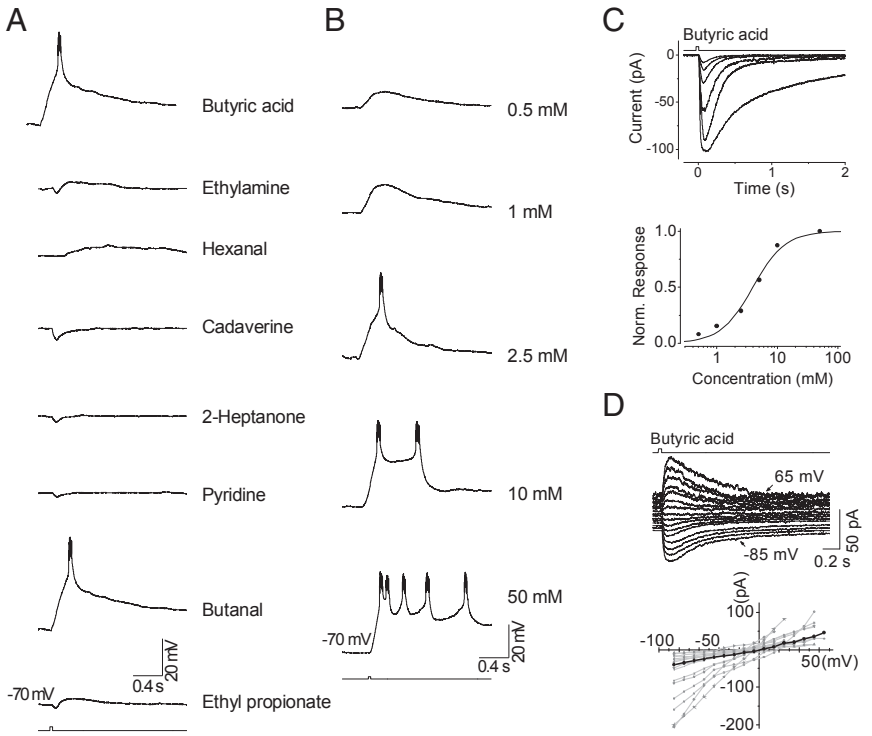

Fig. 3. The odor responses of Ir-expressing OSNs. (*A*) Odor spectrum. Traces show the voltage responses (current clamped) elicited by the indicated odors. Each odor was delivered at 25 mM and applied for 35 ms. (*B*) The dose dependence of spike firing. The same Ir-OSN as that in *A* is shown. Traces show the membrane depolarization elicited by 35-ms pulses of butyric acid at the indicated concentrations. (*C*) The odor response family (*Top*) and dose–response relationship (*Bottom*). A 35-ms pulse of butyric acid at concentrations of 0.5, 1, 2.5, 5, 10, and 50 mM. The curve fit to the dose–response relationship is the Hill equation ($K_{1/2} = 4.0$ mM, $m = 1.6$). (*D*, *Top*) Current–voltage relationship of the response of an OSN to butyric acid (35 ms, 25 mM). The cell is stepped from −85 to 65 mV in 10-mV increments. (*Bottom*) Collected current–voltage relationships from 17 Ir-expressing OSNs, with responses elicited by butyric acid. Black dots (interconnected by straight lines) correspond to data from the OSN at the *Top*.

adaptation is a general feature of Or-expressing OSNs. Interestingly, Or-expressing OSNs with a slow falling phase in their short-pulse responses showed a relatively weaker adaptation.

Next, we investigated adaptation in Ir-expressing OSNs. We recorded receptor currents of ac3A OSNs and found, in contrast, that they did not show adaptation. The receptor current rose and then remained at a steady level during the step stimulation (Fig. 4*E*; $n = 10$). When examined with the paired-pulse protocol, the two pulses triggered identical receptor currents (Fig. 4*F*) at all interpulse intervals tested, further indicating that Ir-expressing OSNs did not adapt. Interestingly, spike firing in these Ir-expressing OSNs did show adaptation. In cell-attached recordings, the recorded OSN fired action potentials at the onset of an odor step, which was followed by a gradual reduction in spike amplitude and even a complete loss of spikes in the presence of a 30-s odor step at a high concentration (Fig. S2*C*). This spike adaptation probably resulted from a change in the spike-generating mechanism, such as the inactivation of voltage-gated sodium channels (34). Similar spike adaptation in Ir-expressing OSNs has been shown in one (15), but not in another (35), study via SSR. In addition, we obtained similar results from OSNs expressing Ir84a (Fig. S2*D*); receptor currents recorded from Ir84a-expressing OSNs did not exhibit adaptation to long steps of phenylacetaldehyde or when probed with paired-pulse stimulations, but spike firing adapted strongly at high odor concentrations.

Changes in Sensitivity and Kinetics During Adaptation. In vertebrate OSNs, the hallmarks of adaptation are a reduction of sensitivity and a prolongation of response kinetics (36–39). We next investigated changes in sensitivity and response kinetics during adaptation in Or22a-expressing OSNs by measuring incremental responses to 35-ms pulses on odor backgrounds. We found that higher concentrations were required to elicit the same criterion response on odor backgrounds, indicating reduced sensitivity in the presence of background odors (Fig. 5 *A* and *B*). Additionally, the amplitude of the saturated response became smaller in the presence of background odors. Notably, a prolongation of the 128 mM ethyl-propionate pulse from 35 to 150 ms was needed to saturate incremental responses in a 4 mM background. In addition to a sensitivity change, background odors also prolonged the time course of odor responses by slowing the receptor current onset (Fig. 5 *C* and *D*).

Voltage and Calcium Dependence of Adaptation. Another striking property of adaptation in *Drosophila* Or-expressing OSNs was its sensitivity to changes in holding potential. The receptor current strongly adapted at a holding potential of −80 mV, but the adaptation was abolished at a holding potential of +40 mV; specifically, the odor-induced receptor current reversed in polarity and then rose and was maintained at a steady level during the 15-s stimulation at a holding potential of +40 mV (Fig. 6*A*). When examined via the paired-pulse protocol, the second pulse triggered a smaller receptor current at −80 mV, but not at +40 mV (Fig. 6*B*).

The voltage dependence of adaptation may be explained by a desensitization triggered by Ca^{2+} entry through nonselective cation transduction channels, which have a reversal potential of approximately −10 mV as noted above (Fig. 1*E*). To investigate a role for Ca^{2+} in OSN adaptation, we first removed all extracellular Ca^{2+}. In the absence of extracellular Ca^{2+}, the receptor current rose and then remained at the same steady level during long-step stimulations, indicating that adaptation had been abolished (Fig. 6*C*, *Bottom*). The removal of extracellular Ca^{2+} also increased the

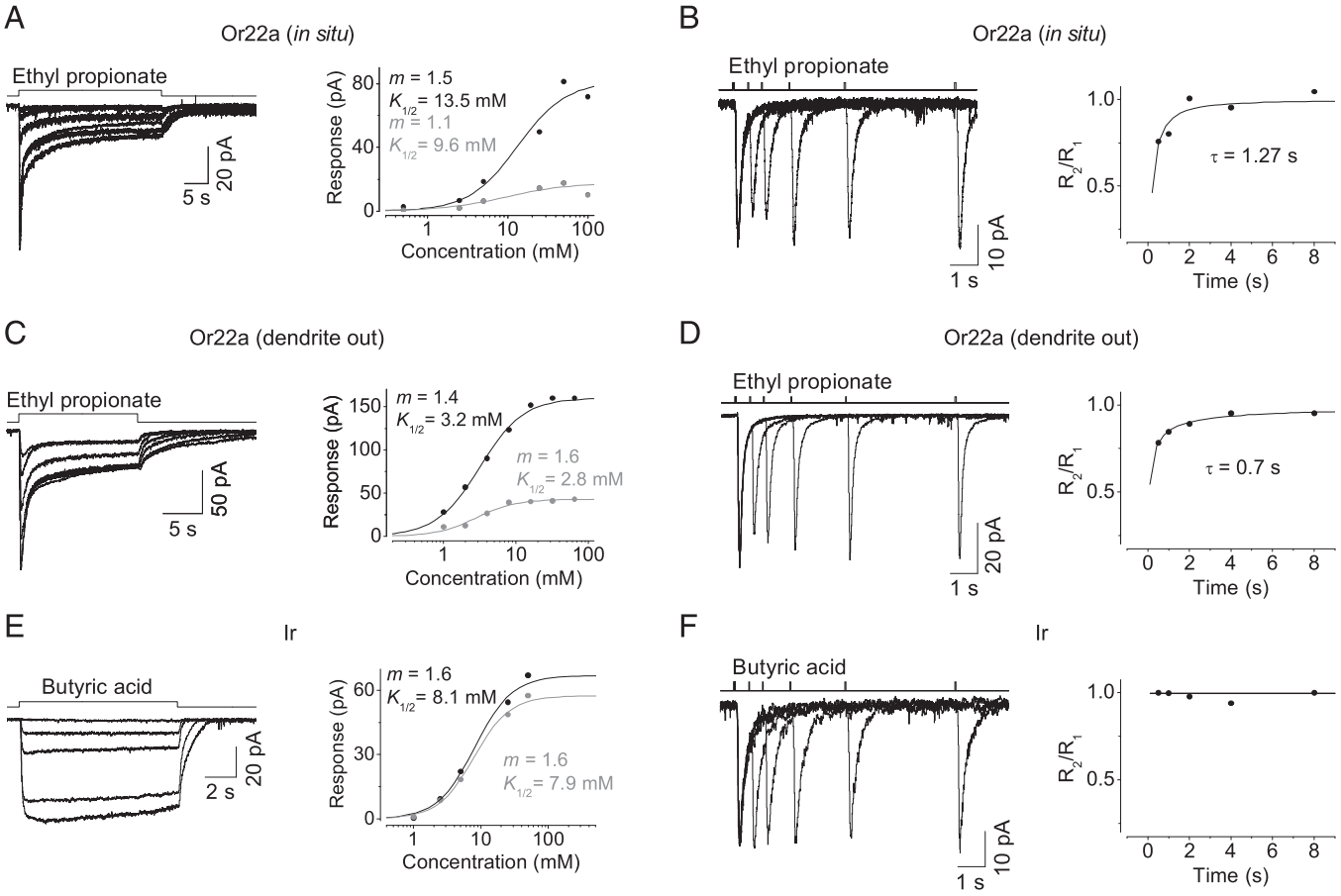

Fig. 4. Adaptation of *Drosophila* OSNs. (*A*) Adaptation in Or22a-expressing OSNs. (*Left*) Receptor current responses to 30-s steps of ethyl propionate at concentrations of 0.5, 2.5, 5, 25, 50, and 100 mM. (*Right*) The dose–response relationship from the response family on the *Left*, with black points representing the receptor current amplitude at transient peaks and the gray points representing the steady state. The curves are derived from the Hill equation, with $K_{1/2}$ = 13.5 and 9.6 mM, m = 1.5 and 1.1, for a transient peak and the steady-state response, respectively. (*B*) Adaptation recovery in Or22a-expressing OSNs. (*Left*) The same OSN as that recorded in *A* showed recovery from adaptation by paired-pulse stimulations at intervals of 0.5, 1, 2, 4, and 8 s. (*Right*) The normalized responses between the two pulses plotted against the intervals. The curve is fit with an exponential function with a time constant of 1.27 s. R_1 and R_2 are the amplitudes of transient-peak responses to the first and second odor pulses, respectively. (*C*) Odor adaptation in Or22a-expressing OSNs with dendrites exposed. (*D*) Adaptation recovery in Or22a-expressing OSNs with dendrites exposed. (*E*) No adaptation was observed in Ir-expressing OSNs. Odor stimulation: 15-s steps of butyric acid at concentrations of 1, 2.5, 5, 30, and 50 mM. (*F*) Responses to paired-pulse stimulation in Ir-expressing OSNs.

receptor current induced by odor steps. For example, the receptor current induced by 8 mM ethyl propionate was threefold larger in the absence of extracellular Ca^{2+} (Fig. 6*C*). Interestingly, a similar increase in response amplitude also occurred for a receptor current triggered by brief pulses (Fig. S3 *A–C*). When extracellular Ca^{2+} was removed, adaptation induced by paired pulses was also abolished, even at negative membrane potentials (Fig. 6*D*). Furthermore, when BAPTA was dialyzed through the electrode into the recorded OSNs to buffer intracellular Ca^{2+}, adaptation was also abolished (Fig. S3*D*), further demonstrating that Ca^{2+} plays a key role in the observed adaptation. Finally, we found that Ca^{2+} released from calcium stores in the endoplasmic reticulum (ER) did not contribute to odor adaptation because similar adaptation existed when the calcium store was depleted via the inhibition of ER Ca^{2+}-ATPase activity with thapsigargin (Fig. S3*E*).

Extension of the Operating Range and Adjustment of Signaling Gain by Adaptation. As shown above, Ca^{2+} entry during an odor response attenuated odor sensitivity, enabling OSNs to avoid saturation. Next, we quantified the changes in sensitivity and operating range during adaptation by adopting a standard protocol used for retinal photoreceptors (29, 40). Specifically, we measured the incremental sensitivity of OSNs to a brief stimulation superimposed on a background stimulus. The OSNs were adapted with an odor step and tested with a superimposed odor pulse (Fig. 7*A*). The pulse concentration was adjusted to trigger a receptor current at ∼10% of the saturated response. The odor sensitivity $S_P{}^B$, defined as the peak response amplitude divided by the incremental odor pulse concentration, progressively decreased with background concentration C_B. Interestingly, we found that the relationship between $S_P{}^B$ and C_B was in accordance with the well-known Weber–Fechner relation, $S_P{}^B/S_p = 1/[1 + (C_B/C_0)]$, where S_p is the sensitivity in the absence of an odor background, and C_0 is the background concentration that halves the OSN's sensitivity (Fig. 7*B*). After abolishing adaptation by removing extracellular Ca^{2+}, the odor sensitivity was higher than that predicted by the Weber–Fechner relation at low backgrounds but dropped sharply at high backgrounds, with a saturating exponential relationship between $S_P{}^B$ and C_B. Thus, as shown in Fig. 7*B*, adaptation in *Drosophila* Or-expressing OSNs extends the operating range of odor concentration by selectively reducing sensitivity at low backgrounds but increasing it at high backgrounds compared with sensitivity in the absence of adaptation. This dynamic sensitivity change differs from the monotonic sensitivity increase incurred upon light adaptation in vertebrate photoreceptors (Fig. 7*C*) (40).

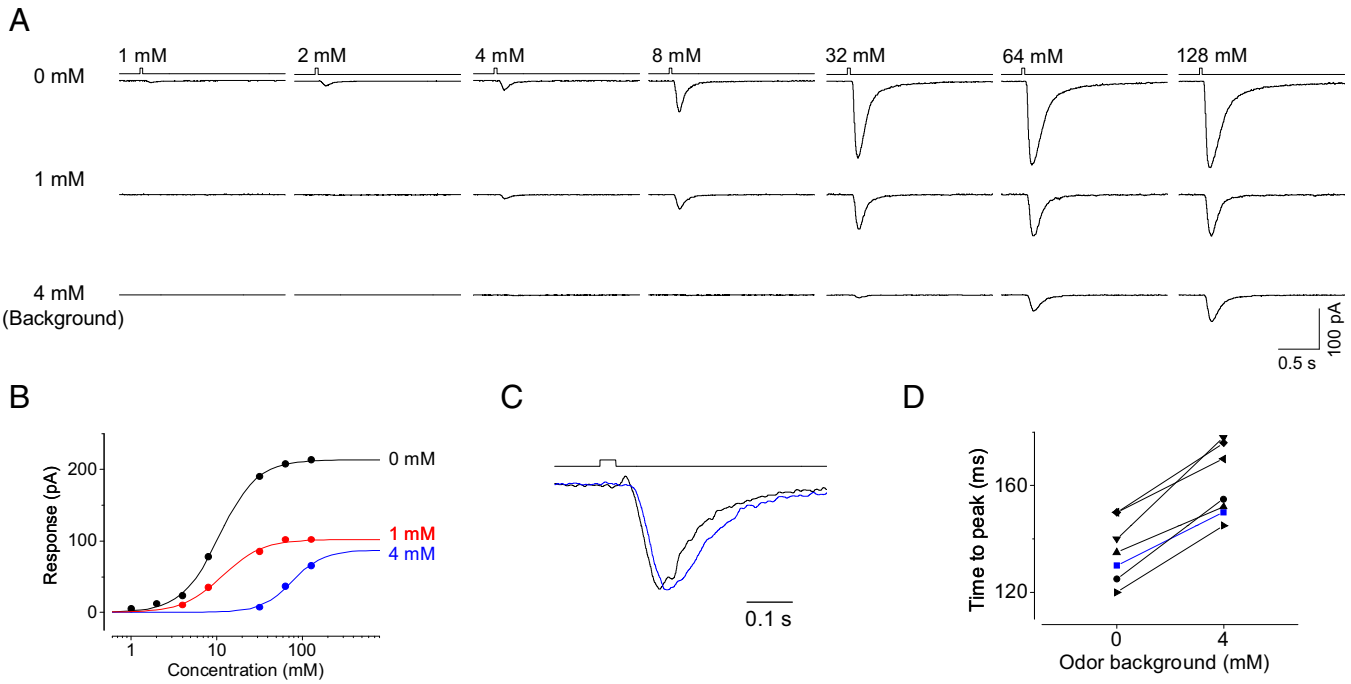

Fig. 5. Changes in the sensitivity and response kinetics by adaptation. (*A*) Incremental responses in Or22a-expressing OSNs to 35-ms pulses of ethyl propionate with no background (*Top*) or 1 mM (*Middle*) and 4 mM (*Bottom*) ethyl propionate backgrounds. (*B*) The dose–response relationship for incremental responses. The peak amplitudes of the incremental responses are plotted against concentrations, with black, red, and green symbols representing data for no background, and 1 and 4 mM ethyl propionate backgrounds, respectively. The background-induced responses are similar to those in Fig. 4 *A* and *C*. (*C*) Changes in the response kinetics by adaptation. Normalized small responses in experiments with and without a 4 mM ethyl propionate background. (*D*) The collective time-to-peak values for weak responses with and without a 4 mM ethyl propionate background.

To understand the effects of adaptation on response sensitivity, we developed a general phenomenological model of sensory adaptation (see *Supporting Information* for details of the model). Our model revealed two opposing effects of adaptation: desensitization and alleviation of saturation (to maintain high sensitivity). At high backgrounds, alleviating saturation dominates over desensitization; therefore, adaptation leads to a higher sensitivity. At low backgrounds, the balance between these effects depends on the strength of adaptation. For a strongly adaptive system such as *Drosophila* Or-expressing OSNs, the desensitization effect of adaptation is relatively strong and leads to a lower sensitivity at low odor concentrations as shown in Fig. 7*C*. However, for a weakly adaptive system such as retinal rod photoreceptors, the desensitization effect is relatively weak, and adaptation increases sensitivity at a low background light intensity (Fig. 7*C*). The trade-off between these two adaptation effects quantitatively explains the difference in sensitivity change between vertebrate photoreceptors and *Drosophila* Or-expressing OSNs (Fig. 7*C* and *Discussion*).

Discussion

Despite the popularity of *Drosophila* as a model organism in olfactory research, the cellular signaling and physiology of its OSNs remain largely unclear. An attempt has previously been made to obtain patch-clamp recordings of single *Drosophila* OSNs (41), but the low yield of this blind recording approach, which does not enable visualization of the recorded OSNs, and the absence of robust odor responses have been major drawbacks. The technical challenge of developing a targeted recording method is mainly imposed by the small size of the peripheral olfactory organs, the cuticle encasing the olfactory tissue, and the sheath cells wrapping the OSNs. Here, we developed an antennal preparation by cutting the third antenna into transverse slices to expose the somata of OSNs. With this preparation, we were able to perform patch-clamp recordings of single visualized *Drosophila* OSNs after mechanically removing the surrounding sheath cells.

In this study, we provided a comprehensive characterization of the basic properties of odor-induced receptor currents in *Drosophila* OSNs. For brief-pulse stimulations, we found that the Or-mediated receptor current had a longer response latency and time-to-peak compared with the Ir responses. When examined during exposure to long-step odors, the receptor current of *Drosophila* Ir-expressing OSNs did not adapt. In contrast, *Drosophila* Or-expressing OSNs strongly adapted, consistently with the LFP studies using either EAG or SSR (19, 24, 42). Furthermore, *Drosophila* Or-expressing OSNs with a sensory dendrite inside or outside the sensillar cavity exhibited similar adaptation, indicating that the cellular mechanisms intrinsic to OSNs rather than lymph-related factors produce the adaptation. Interestingly, *Drosophila* Or-expressing OSNs share similar adaptation features with vertebrate OSNs, despite possible differences in odor transduction mechanisms (43). For example, as in vertebrate OSNs (37, 44), the steady-state receptor current in *Drosophila* Or-expressing OSNs during adaptation can reach less than 20% of the transient peak response. Also similarly to vertebrate OSNs (37, 38), adaptation reduced the sensitivity and slowed the response kinetics of *Drosophila* Or-expressing OSNs, consistently with LFP studies using SSR (24). Furthermore, we found that adaptation in *Drosophila* Or-expressing OSNs was mediated by the Ca^{2+} influx during odor responses, as is that in vertebrate OSNs (36, 38).

What are the molecular targets of Ca^{2+} effects during odor adaptation? In vertebrate OSNs, several mechanisms have been proposed, including the desensitization of transduction channels, phosphorylation of odorant receptors, inhibition of adenylyl cyclase, and potentiation of phosphodiesterase activity (37, 38, 45). Recent molecular genetic studies have revealed, however, that adaptation in vertebrate OSNs is more complex than previously

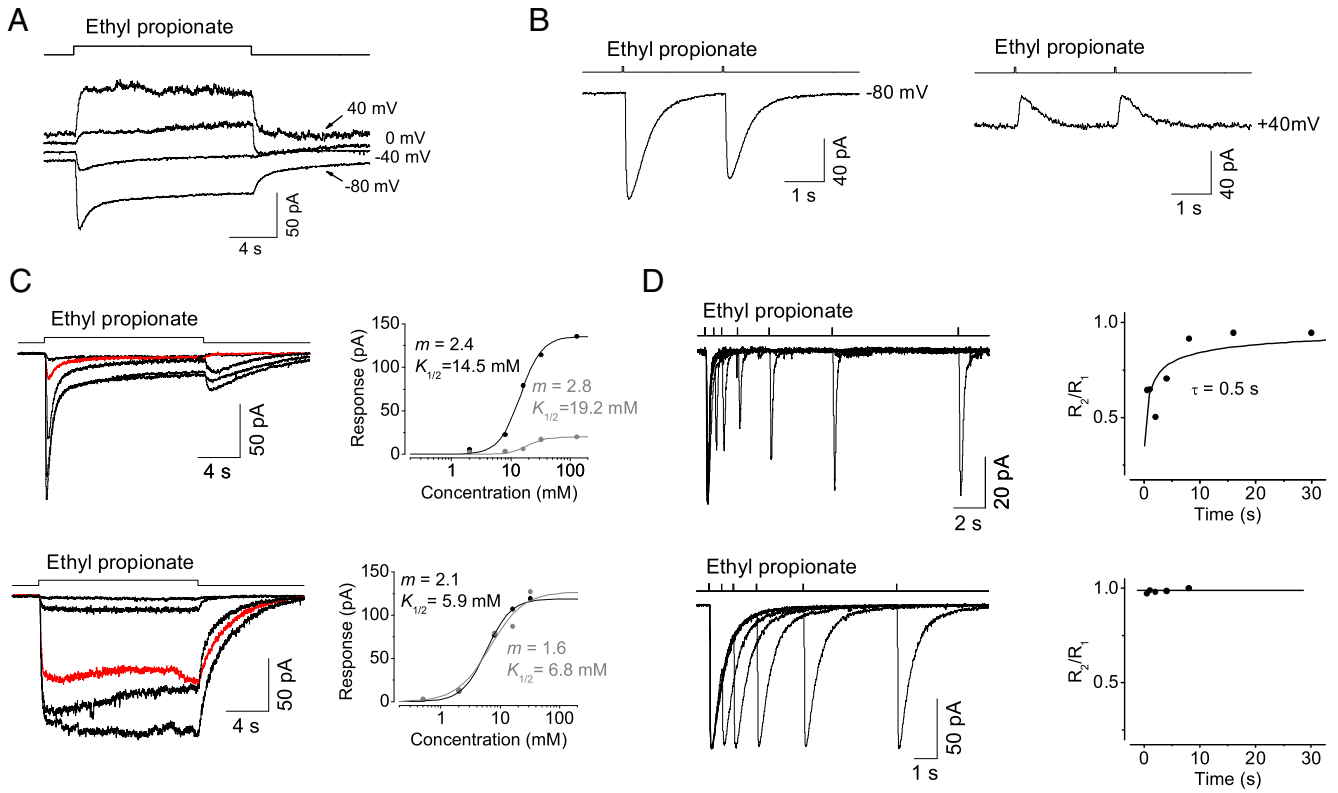

Fig. 6. The voltage and Ca^{2+} dependence of adaptation. (*A*) The voltage dependence of step adaptation. Odor stimulation: 20-s steps of 50 mM ethyl propionate. Holding potentials are as indicated. (*B*) The voltage dependence of paired-pulse responses. Left and right panels were obtained from the same OSN. Odor stimulation: 35-ms pulses of 50 mM ethyl propionate at an interval of 4 s. Holding potentials at −80 mV (*Left*) and +40 mV (*Right*). Note the abolishment of the reduction in second-pulse–triggered receptor current at +40 mV. (*C*) The Ca^{2+} dependence of step adaptation. The top and bottom panels are from the same OSN. Adaptation (*Left, Top*) is abolished after removing extracellular Ca^{2+} (*Left, Bottom*), with traces for 8 mM ethyl propionate marked in red. (*Right*) The dose–response relationships at a transient peak and in the steady state are represented with black and gray symbols, respectively. (*D*) The Ca^{2+} dependence of paired-pulse adaptation. Top and bottom panels were obtained from the same OSN. Odor stimulation: 35-ms pulses of 50 mM ethyl propionate. Note that adaptation (*Left, Top*) is abolished when extracellular Ca^{2+} is removed (*Left, Bottom*). The response ratio at transient peaks between the two pulses plotted against the intervals (*Right*).

understood (46, 47). To date, the odor transduction mechanism in *Drosophila* OSNs remains unclear, although heterologous studies have suggested novel and controversial mechanisms (43). However, the observed differences in responses kinetics and adaptation properties between Or- and Ir-OSNs suggest that the two types of neurons may use distinct odor transduction mechanisms. Alternatively, if both Or and Ir were ionotropic, the activation of Or and Ir would have to be different. If G-protein signaling is involved in generating odor responses in *Drosophila* Or-expressing OSNs, the targets of Ca^{2+} modulation could be any component ranging from Ors to transduction channels as in vertebrate OSNs. Otherwise, Ors/Orco would be the target of Ca^{2+} modulation during adaptation in *Drosophila* Or-expressing OSNs. Future studies are required to fully elucidate the mechanisms of Ca^{2+}-mediated adaptation in *Drosophila* OSNs as well as in vertebrate OSNs.

Odor sensitivity in *Drosophila* Or-expressing OSNs adapts to the odor background in accordance with the Weber–Fechner relation, which is well known for describing the adaptation of retinal photoreceptors (40, 48). In the absence of extracellular Ca^{2+}, the Weber–Fechner relation no longer held and was replaced by a saturating exponential relationship with a concomitant reduction in the operating range. Interestingly, the two mathematical relationships intersect at a background concentration, revealing that adaptation selectively reduces sensitivity at a low background but increases sensitivity at a high background. This dynamic adjustment of sensitivity during adaptation is in great contrast to the long-held view that adaptation always increases sensitivity as has been established for vertebrate photoreceptors (40, 48).

Motivated by the observed difference in sensitivity change, we developed a general mathematical framework to understand the response of sensory systems with and without adaptation (*Supporting Information*). The results of our model reveal a trade-off between two adaptation effects: (*i*) desensitization to reduce odor sensitivity and (*ii*) alleviation of saturation to increase sensitivity. At high backgrounds, adaptation prevents the sensory system from reaching saturation, in which sensitivity drops exponentially. As a result, adaptation leads to a higher sensitivity in all sensory systems at high backgrounds (Fig. 7*C*). At low backgrounds, the sensory system is not close to saturation; thus, the desensitization effect of adaptation can become dominant. For a strongly adaptive system such as the *Drosophila* Or-expressing OSNs, this desensitization effect is strong and leads to a lower sensitivity at low background odor concentrations. In contrast, in retinal rod photoreceptors, adaptation increases sensitivity at all background light intensities (40, 48). This difference can be explained by the relatively weak adaptation of retinal photoreceptors; thus, the increase in sensitivity caused by the alleviation of saturation dominates desensitization at all backgrounds (*Supporting Information*). Similarly to *Drosophila* Or-expressing OSNs, sensory neurons in many other modalities, such as hair cells (49), exhibit strong adaptation. Thus, understanding of the dynamic sensitivity adjustment by odor adaptation in *Drosophila* may serve as a guiding principle for understanding the effects of

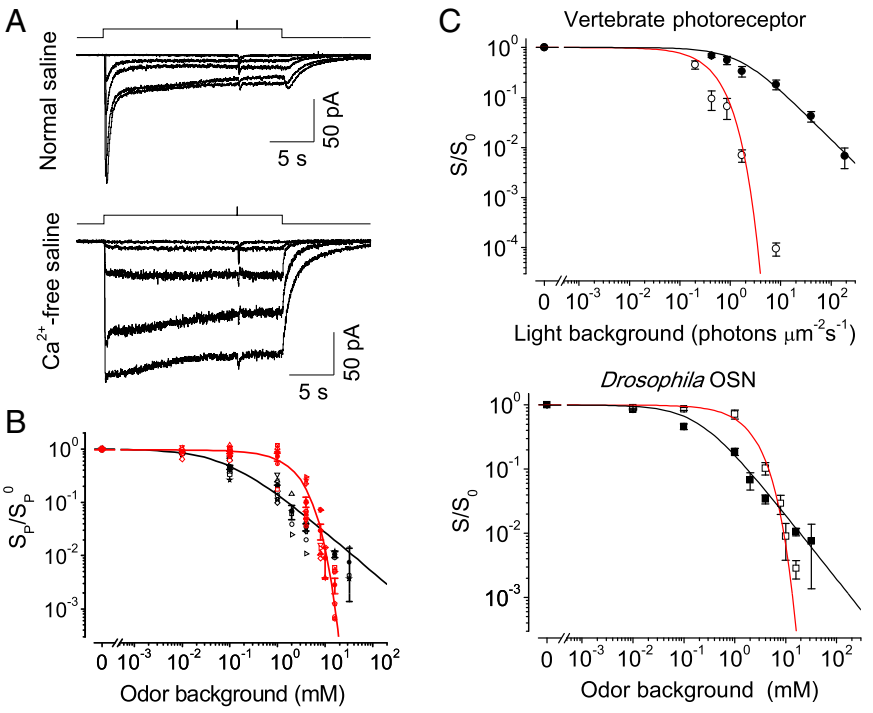

Fig. 7. Gain control during adaptation. (*A*) Incremental sensitivity under background adaptation. The top and bottom panels were obtained from the same OSN. Odor backgrounds: 20-s steps of ethyl propionate at various concentrations. Incremental pulses: 35-ms pulses of ethyl propionate at various concentrations. Normal saline (*Top*) and Ca^{2+}-free saline (*Bottom*). (*B*) The normalized odor sensitivity against background concentrations. Black and red symbols represent data in the presence and absence of extracellular Ca^{2+}, respectively. The fit in black represents the Weber–Fechner relation, $S_P^B/S_P = 1/[1 + (C_B/C_0)]$ with $C_0 = 0.09$ mM; the fit in red represents the saturating exponential function, $S_P^B/S_P = \exp(-kC_B)$, where k is a constant of 0.4 mM^{-1}. (*C*) Model results and experimental data. (*Top*) The normalized photosensitivity of vertebrate photoreceptors, with data points extracted from figure 2b in ref. 40. (*Bottom*) The same data as that shown in *B* for *Drosophila* OSNs. The red curves are fit with $S/S_0 = \exp(-u_0/K_{NA})$, and the black curves are fit with $S/S_0 = \exp[-u_0/(K_0 + \alpha u_0)] \times [K_0/(K_0 + \alpha u_0)]$, with parameters specified in Fig. S4.

adaptation in other senses. With respect to modeling, it remains a challenge to understand the general effects of adaptation according to the underlying molecular mechanisms in sensory neurons (50), as has been done in the simpler case of bacterial chemotaxis (51).

The ability of strong adaptation by Ors would allow *Drosophila* to track odor changes over a broad range of concentrations and to detect other odors even in the presence of certain background odor. In contrast, without the ability to adapt, Irs are better suited for detecting absolute odor concentrations, allowing *Drosophila* to efficiently locate food, mates, or predators.

Materials and Methods

Fly Stocks. All flies were raised on standard cornmeal agar medium, under 60% humidity and a 12-h light/12-h dark cycle at 25 °C. The *Orco-Gal4*, *Or47a-Gal4*, *Or22a-Gal4*, and *Orco*^{2} flies were obtained from the Bloomington Stock Center and had been deposited by Dr. Leslie B. Vosshall, Rockefeller University, New York. *UAS-mCD8-GFP* flies were obtained from the same center and had been deposited by Dr. Liqun Luo, Stanford University, Stanford, CA. *Ir84a*-Gal4 was a gift from Dr. Richard Benton, University of Lausanne, Lausanne, Switzerland.

Preparation. Young adult flies (1–4 d after eclosion) were immobilized on ice. The decapitated heads were transferred into dissection solution. The third segment of an antenna was isolated and cut into three transverse pieces (slices), each ∼50 μm thick. The antennal slice was stabilized in the recording chamber with vacuum grease, with one cut end facing up and continuously bath-perfused with 95% O_2/5% (vol/vol) CO_2-bubbled *Drosophila* saline. Each OSN in the antenna projects a dendrite from the cell body into a sensillum. On average, ∼20 intact OSNs could be found in the top layer of a slice, whereas the others (∼10) typically had damaged dendrites, cell bodies, or sensilla. Below the top layer at the open end, most OSNs were intact. Patch-clamp recordings could be made from OSNs in the top three layers.

Solutions and Electrical Recordings. *Drosophila* saline contained the following (in mM): 158 NaCl, 3 KCl, 4 $MgCl_2$, 1.5 $CaCl_2$, 26 $NaHCO_3$, 1 NaH_2PO_4, 5 *N*-tri (hydroxymethyl)-methyl-2-aminoethane-sulfonic acid (TES), 10 D-glucose, 17 sucrose, and 5 trehalose, bubbled with 95% O_2/5% CO_2 (pH 7.4). The osmolality was ∼400 mOsm and has been found to be critical for the health of OSNs and for eliciting stable odor responses (up to 2 h). The dissection solution was made by replacing $NaHCO_3$, NaH_2PO_4, and TES in *Drosophila* saline with 5 mM 4-(2-hydroxyethl)-1-piperazineethanesulfonic acid (Hepes) and 27 mM NaCl (pH 7.4, adjusted with NaOH), bubbled with oxygen. All chemicals, including odors, were obtained from Sigma-Aldrich. Odors were freshly dissolved in *Drosophila* saline daily within their water solubility. The pH of odor solutions was not corrected. For example, the pH values of 1 and 50 mM butyric acid solutions are ∼7.10 and 4.40, respectively. Tetraethyl ammonium chloride (TEA), 4-aminopyridine (4-AP), and thapsigargin were also obtained from Sigma-Aldrich, and tetrodotoxin (TTX) was obtained from Alomone Labs. All reagents were directly dissolved in *Drosophila* saline, with the exception of thapsigargin, which was dissolved in dimethyl sulfoxide (DMSO).

OSNs in the antennal slice were visualized on an upright microscope (Scientifica), with infrared–differential interference contrast (IR-DIC) optics and a 60× water-immersion objective (Olympus). The image was captured with an IR-CCD (DAGE-MTI) and displayed on a television monitor (Sony). Patch-clamp recordings were made with MultiClamp 700B (Molecular Devices). The patch electrodes were made from borosilicate glass (WPI) with a P-97 puller (Sutter). The OSNs in the *Drosophila* antenna are small, with cell bodies of only 3–5 μm in diameter, requiring a recording pipette tip of ∼0.2 μm and a resistance of ∼20 MΩ when filled with intracellular saline (in mM: 185 K-gluconate, 5 NaCl, 2 $MgCl_2$, 0.1 $CaCl_2$, 1 EGTA, 10 Hepes; pH 7.4; ∼390 mOsm). Typically, a seal of 2–8 GΩ between OSN membrane and a patch-clamp pipette could be obtained. For perforated patch-clamp recordings, amphotericin B was dissolved in DMSO, then diluted with intracellular saline to a final concentration of 200 μg/mL, and backfilled into the recording pipette. For whole-cell patch-clamp recordings, GTP-Tris (0.5 mM) and Mg-ATP (4 mM) were added to the intracellular saline. For cell-attached recordings, the recording pipette was filled with dissection solution. To measure the current–voltage relationship, voltage-sensitive Na channels and K channels were blocked by a mixture of TTX (50 nM), TEA (10 mM), and sometimes also 4-AP (10 mM). In experiments requiring the removal of extracellular Ca^{2+}, the perfusion saline was composed of the following (in mM): 158 NaCl, 3 KCl, 7.6 $MgCl_2$, 26 $NaHCO_3$, 1 NaH_2PO_4, 10 EGTA, 5 TES, 10 D-glucose, 17 sucrose, and 5 trehalose, bubbled with 95% O_2/5% CO_2 (pH 7.4). Current and voltage signals were digitized and recorded with Digidata 1440A and pClamp 10.2 (Molecular Devices), filtered at 2 kHz, and sampled at 5 kHz. Recorded currents were low-pass filtered at 200 Hz (unless stated otherwise) for display, introducing a ∼3-ms peak delay compared with low-pass filtering at 2 kHz. The voltage was clamped at −80 mV unless stated otherwise. Measured voltages were corrected for a liquid junction potential.

Odor Stimulation. Rapid solution changes were produced by translating the interface between the two flowing solution streams across the recorded OSN with an electronic stepper (Warner Instruments) attached to a three-barrel tube (Warner Instruments), with the tip positioned ∼50 μm away from an

antennal slice. Each barrel was connected to an 8-to-1 manifold. Thus, a total of 24 solutions could be used. The solution flow was driven by gravity at a speed of ~16 mm·s^{-1} at the tubing tip and was controlled by solenoid valves (The Lee Company) and a valve controller (AutoMate Scientific). The inner width of each square barrel of the perfusion tubing was 600 μm, emitting a solution readily covering the antennal slice (~50 μm thick, ~40 μm wide, and ~70 μm long).

Dendrite-Out Preparation. Typically, the dendrite of an OSN consists of an inner dendrite housed in the antennae and an outer dendrite in the sensillum. The outer (or sensory) dendrite is thus immersed in sensillar lymph. To rule out contributions of factors in the sensillar lymph to the odor responses of OSNs, we developed a dendrite-out preparation. Before patch-clamp recording, the sensory dendrite of a targeted OSN was pulled out from its sensillar cavity, by using a glass pipette with a tip opening of ~2 μm to suck the inner dendrites and then mechanically pull out the sensory dendrites from the sensillar cavity. As a result, the sensory dendrite of the targeted OSN was immersed in the bath perfusion solution rather than in the sensillar lymph.

Measurements of Response Latency. The time delay between the voltage trigger driving the electronic stepper and the appearance of an electrical response is due to the following: (*i*) the time required for the stepper-driven mechanical translation of the three-barrel tubing, (*ii*) the travel time for the odor solution to reach the antennal slice, (*iii*) the time required for odorant molecules to penetrate the pores in the sensillum and reach the OSN dendrite by diffusion, and (*iv*) the time delay in olfactory transduction (i.e., response latency). The first two delays were measured to be 28 ms, based on liquid-junction current measurements (Fig. S1*G*). The third delay has been estimated by others to be ~5 ms (1). Thus, the response latency ($t_{latency}$) is obtained by subtracting 33 ms (28 + 5 ms) from the total response delay.

ACKNOWLEDGMENTS. We thank King-Wai Yau, Jeremy Nathans, Trevor D. Lamb, Christopher J. Potter, and Karl-Ernst Kaissling for discussions; Wendy W.-S. Yue and Minmin Luo for comments on the manuscript; and Alex Kolodkin, Adrienne Dubin, Baruch Minke, and Vikas Bhandawat for technical advice and help. The work was supported by National Natural Science Foundation of China Grant 31471053, the Ministry of Education [the Young Thousand Talent Program (D.-G.L.)], the Peking–Tsinghua Center for Life Sciences, the Center for Quantitative Biology, the State Key Laboratory of Membrane Biology, and the College of Life Sciences at Peking University. Y.T. was supported by NIH Grant R01GM081747, and Y.S. was supported by National Natural Science Foundation of China Grant 31471024 and Natural Science Foundation of Zhejiang Province (Grant Z15C090001).

1. Kaissling KE (1986) Chemo-electrical transduction in insect olfactory receptors. *Annu Rev Neurosci* 9:121–145.
2. Prasad BC, Reed RR (1999) Chemosensation: Molecular mechanisms in worms and mammals. *Trends Genet* 15(4):150–153.
3. Firestein S (2001) How the olfactory system makes sense of scents. *Nature* 413(6852): 211–218.
4. Ache BW, Young JM (2005) Olfaction: Diverse species, conserved principles. *Neuron* 48(3):417–430.
5. Kleene SJ (2008) The electrochemical basis of odor transduction in vertebrate olfactory cilia. *Chem Senses* 33(9):839–859.
6. Ma M (2012) Odor and pheromone sensing via chemoreceptors. *Adv Exp Med Biol* 739:93–106.
7. Vosshall LB, Stocker RF (2007) Molecular architecture of smell and taste in *Drosophila*. *Annu Rev Neurosci* 30:505–533.
8. Benton R (2008) Chemical sensing in *Drosophila*. *Curr Opin Neurobiol* 18(4):357–363.
9. Su CY, Menuz K, Carlson JR (2009) Olfactory perception: Receptors, cells, and circuits. *Cell* 139(1):45–59.
10. Hallem EA, Ho MG, Carlson JR (2004) The molecular basis of odor coding in the *Drosophila* antenna. *Cell* 117(7):965–979.
11. Hallem EA, Carlson JR (2006) Coding of odors by a receptor repertoire. *Cell* 125(1): 143–160.
12. Fishilevich E, Vosshall LB (2005) Genetic and functional subdivision of the *Drosophila* antennal lobe. *Curr Biol* 15(17):1548–1553.
13. Couto A, Alenius M, Dickson BJ (2005) Molecular, anatomical, and functional organization of the *Drosophila* olfactory system. *Curr Biol* 15(17):1535–1547.
14. Benton R, Vannice KS, Gomez-Diaz C, Vosshall LB (2009) Variant ionotropic glutamate receptors as chemosensory receptors in *Drosophila*. *Cell* 136(1):149–162.
15. Abuin L, et al. (2011) Functional architecture of olfactory ionotropic glutamate receptors. *Neuron* 69(1):44–60.
16. Silbering AF, et al. (2011) Complementary function and integrated wiring of the evolutionarily distinct *Drosophila* olfactory subsystems. *J Neurosci* 31(38):13357–13375.
17. Rytz R, Croset V, Benton R (2013) Ionotropic receptors (IRs): Chemosensory ionotropic glutamate receptors in *Drosophila* and beyond. *Insect Biochem Mol Biol* 43(9): 888–897.
18. Keil TA, Steiner C (1991) Morphogenesis of the antenna of the male silkmoth. *Antheraea polyphemus*, III. Development of olfactory sensilla and the properties of hair-forming cells. *Tissue Cell* 23(6):821–851.
19. Störtkuhl KF, Hovemann BT, Carlson JR (1999) Olfactory adaptation depends on the Trp Ca^{2+} channel in *Drosophila*. *J Neurosci* 19(12):4839–4846.
20. Siddiqi O (1987) Neurogenetics of olfaction in *Drosophila melanogaster*. *Trends Genet* 3:137–142.
21. Clyne P, Grant A, O'Connell R, Carlson JR (1997) Odorant response of individual sensilla on the *Drosophila* antenna. *Invert Neurosci* 3(2-3):127–135.
22. Pellegrino M, Nakagawa T, Vosshall LB (2010) Single sensillum recordings in the insects *Drosophila melanogaster* and *Anopheles gambiae*. *J Vis Exp* 36:1–5.
23. Benton R, Dahanukar A (2011) Electrophysiological recording from *Drosophila* olfactory sensilla. *Cold Spring Harb Protoc* 2011(7):824–838.
24. Nagel KI, Wilson RI (2011) Biophysical mechanisms underlying olfactory receptor neuron dynamics. *Nat Neurosci* 14(2):208–216.
25. Kaissling KE (1995) Single unit and electroantennogram recordings in insect olfactory organs. *Experimental Cell Biology of Taste and Olfaction. Current Techniques and Protocols*, eds Spielman AI, Brand JG (CRC, Boca Raton, FL), pp 361–377.
26. Larsson MC, et al. (2004) *Or83b* encodes a broadly expressed odorant receptor essential for *Drosophila* olfaction. *Neuron* 43(5):703–714.
27. Firestein S, Picco C, Menini A (1993) The relation between stimulus and response in olfactory receptor cells of the tiger salamander. *J Physiol* 468:1–10.
28. Bhandawat V, Reisert J, Yau KW (2010) Signaling by olfactory receptor neurons near threshold. *Proc Natl Acad Sci USA* 107(43):18682–18687.
29. Luo DG, Kefalov V, Yau KW (2008) Phototransduction in retinal rods and cones. *The Senses—A Comprehensive Reference*, eds Masland RH, Albridght TD (Elsevier, New York), Vol 1, pp 269–301.
30. Cao LH, Luo DG, Yau KW (2014) Light responses of primate and other mammalian cones. *Proc Natl Acad Sci USA* 111(7):2752–2757.
31. Su CY, Menuz K, Reisert J, Carlson JR (2012) Non-synaptic inhibition between grouped neurons in an olfactory circuit. *Nature* 492(7427):66–71.
32. Yao CA, Ignell R, Carlson JR (2005) Chemosensory coding by neurons in the coeloconic sensilla of the *Drosophila* antenna. *J Neurosci* 25(37):8359–8367.
33. Kurahashi T, Lowe G, Gold GH (1994) Suppression of odorant responses by odorants in olfactory receptor cells. *Science* 265(5168):118–120.
34. Kaissling KE, Zack Strausfeld C, Rumbo ER (1987) Adaptation processes in insect olfactory receptors. Mechanisms and behavioral significance. *Ann N Y Acad Sci* 510: 104–112.
35. Getahun MN, Wicher D, Hansson BS, Olsson SB (2012) Temporal response dynamics of *Drosophila* olfactory sensory neurons depends on receptor type and response polarity. *Front Cell Neurosci* 6:54.
36. Kurahashi T, Shibuya T (1990) Ca^{2+}-dependent adaptive properties in the solitary olfactory receptor cell of the newt. *Brain Res* 515(1-2):261–268.
37. Leinders-Zufall T, Ma M, Zufall F (1999) Impaired odor adaptation in olfactory receptor neurons after inhibition of Ca^{2+}/calmodulin kinase II. *J Neurosci* 19(14): RC19.
38. Reisert J, Matthews HR (1999) Adaptation of the odour-induced response in frog olfactory receptor cells. *J Physiol* 519(Pt 3):801–813.
39. Boccaccio A, Lagostena L, Hagen V, Menini A (2006) Fast adaptation in mouse olfactory sensory neurons does not require the activity of phosphodiesterase. *J Gen Physiol* 128(2):171–184.
40. Matthews HR, Murphy RL, Fain GL, Lamb TD (1988) Photoreceptor light adaptation is mediated by cytoplasmic calcium concentration. *Nature* 334(6177):67–69.
41. Dubin AE, Harris GL (1997) Voltage-activated and odor-modulated conductances in olfactory neurons of *Drosophila melanogaster*. *J Neurobiol* 32(1):123–137.
42. Martelli C, Carlson JR, Emonet T (2013) Intensity invariant dynamics and odor-specific latencies in olfactory receptor neuron response. *J Neurosci* 33(15):6285–6297.
43. Nakagawa T, Vosshall LB (2009) Controversy and consensus: Noncanonical signaling mechanisms in the insect olfactory system. *Curr Opin Neurobiol* 19(3):284–292.
44. Firestein S, Shepherd GM, Werblin FS (1990) Time course of the membrane current underlying sensory transduction in salamander olfactory receptor neurones. *J Physiol* 430:135–158.
45. Kurahashi T, Menini A (1997) Mechanism of odorant adaptation in the olfactory receptor cell. *Nature* 385(6618):725–729.
46. Song Y, et al. (2008) Olfactory CNG channel desensitization by Ca^{2+}/CaM via the B1b subunit affects response termination but not sensitivity to recurring stimulation. *Neuron* 58(3):374–386.
47. Cygnar KD, Collins SE, Ferguson CH, Bodkin-Clarke C, Zhao H (2012) Phosphorylation of adenylyl cyclase III at serine^{1076} does not attenuate olfactory response in mice. *J Neurosci* 32(42):14557–14562.
48. Pugh EN, Jr, Nikonov S, Lamb TD (1999) Molecular mechanisms of vertebrate photoreceptor light adaptation. *Curr Opin Neurobiol* 9(4):410–418.
49. Peng AW, Effertz T, Ricci AJ (2013) Adaptation of mammalian auditory hair cell mechanotransduction is independent of calcium entry. *Neuron* 80(4):960–972.
50. De Palo G, et al. (2013) Common dynamical features of sensory adaptation in photoreceptors and olfactory sensory neurons. *Sci Rep* 3:1251.
51. Tu Y (2013) Quantitative modeling of bacterial chemotaxis: Signal amplification and accurate adaptation. *Annu Rev Biophys* 42:337–359.
52. Kaissling KE (1998) Flux detectors versus concentration detectors: Two types of chemoreceptors. *Chem Senses* 23(1):99–111.
53. Zhou Y, Wilson RI (2012) Transduction in *Drosophila* olfactory receptor neurons is invariant to air speed. *J Neurophysiol* 108(7):2051–2059.